Figure S1

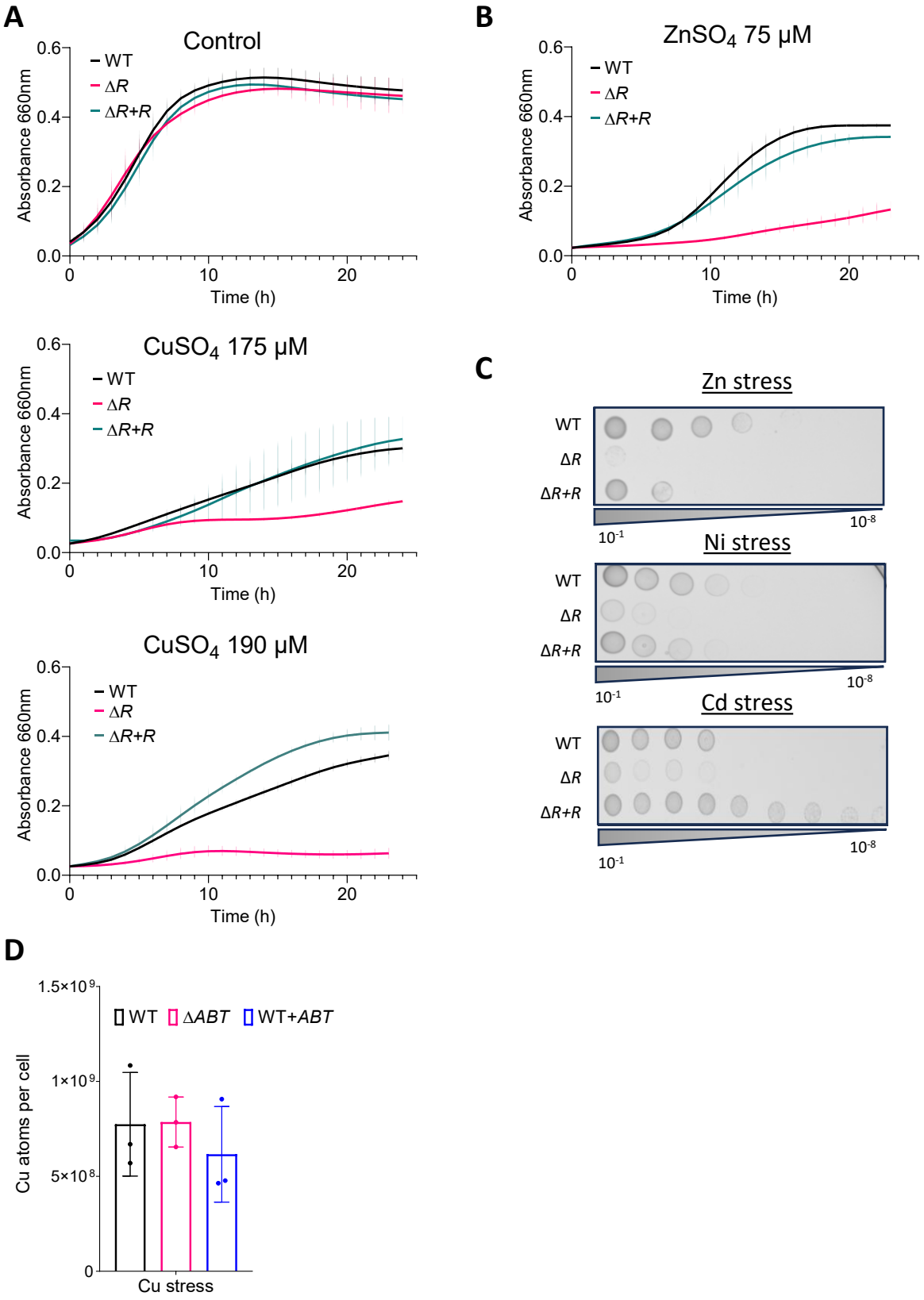

Figure S1: Cu sensitivity of the Δ*R* mutant is not Cu-specific. A. Growth profiles at an OD_{660} nm of WT, Δ*R*, and Δ*R+R* strains in control PYE medium and supplemented with 175 µM and 190 µM $CuSO_4$. **B.** Growth profiles at an OD_{660} nm of WT, Δ*R*, and Δ*R+R* strains in control PYE medium supplemented with 75 µM of $ZnSO_4$. **C.** Viability assay on PYE plates of WT, Δ*R*, and Δ*R+R* strains, in 50 µM $ZnSO_4$, 200 µM $NiSO_4$ and 2 µM $CdSO_4$ conditions. **D.** Number of Cu atoms per cell exposed to 175 µM $CuSO_4$ excess for 5 min. All data are represented as the mean ± SD, with at least three biological replicates.

Figure S2

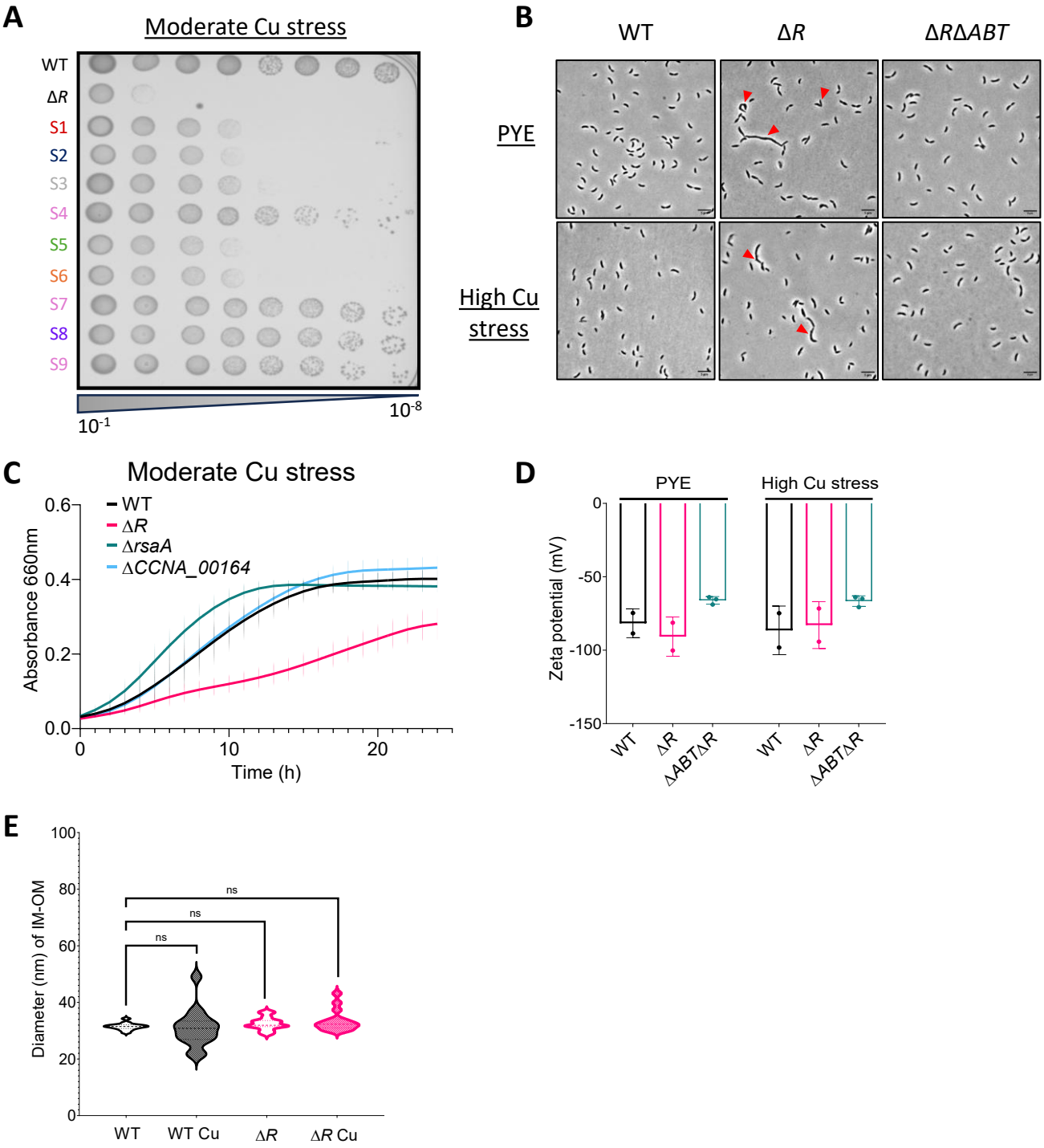

Figure S2: Microscopic and genetic analysis of cell surface alterations and their Impact on Cu sensitivity. A. Suppressors of the Δ*R* mutant were found on PYE plates supplemented with 120 µM $CuSO_4$. In total, 9 suppressors were isolated, which to some extent showed improved growth on Cu compared to the Δ*R* mutant. **B.** Phase-contrast microscopy images of WT, Δ*R*, and Δ*R*Δ*ABT* strains at exponential phase in control condition and exposed for 1 h to 190 µM $CuSO_4$ (bar = 5 µm). **C**. Growth profiles at an OD_{660} nm of WT, Δ*R*, Δ*rsaA*, and Δ*CCNA_00164* strains PYE medium supplemented with 150 µM $CuSO_4$. All data are represented as the mean ± SD, with at least three biological replicates. **D.** Zeta potential measurements of WT, Δ*R*, and Δ*R*Δ*ABT* cells with or without 190 µM $CuSO_4$ treatment. Mean ± SD, at least two biological replicates. **E.** Diameter of the distance between OM-IM space from Cyro-EM images. Distribution of OM-IM diameter space quantified from Cryo-EM microscopy images of WT and Δ*R* strains at exponential phase in control condition and exposed for 1 h to 190 µM $CuSO_4$. The solid line indicates the median, broken lines represent the 25th and 75th percentiles, respectively.

Figure S3

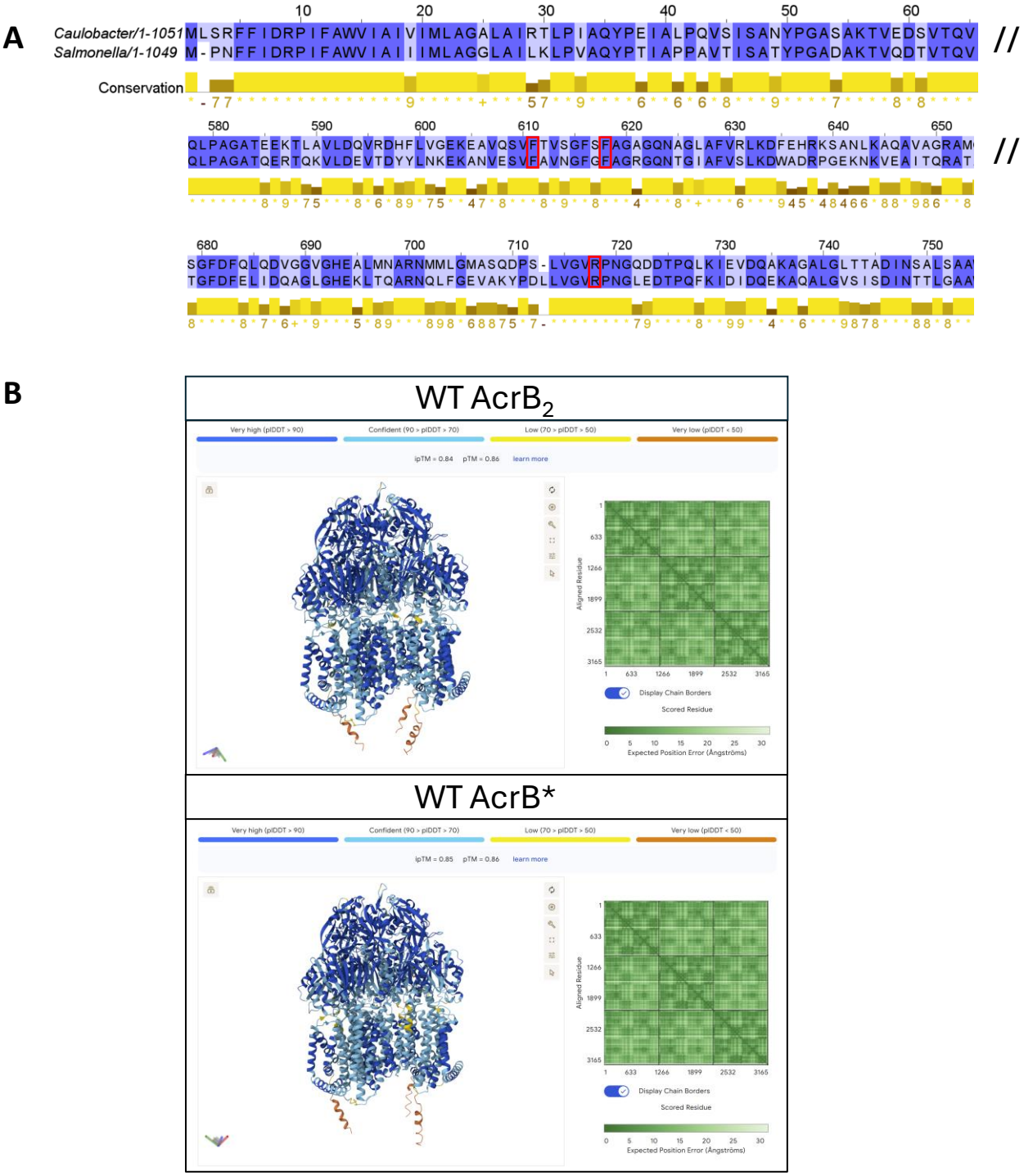

Figure S3: Multiple sequence alignment of $AcrB_2$ and AlphaFold3 prediction. A. Multiple MAFFT alignment of $AcrB_{Cv}$ with AcrB homologs from *Salmonella typhimurium*. Identical residues are highlighted in blue, and the three conserved amino acids of interest, F610, F617, and R716, are highlighted in red. **B.** Graphic plot of the prediction of $AcrB_{cv}$ and $AcrB_{cv}$* accounting for the pLDDT and PAE (source AlphaFold3).

Figure S4

A

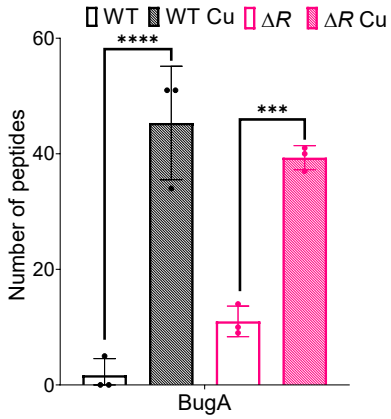

Figure S4: Protein abundance of BugA. A. Normalized total spectrum count of BugA protein in PYE medium, in combination with a 1 h exposure to 190 µM $CuSO_4$. All data are represented as the mean ± SD, with at least three biological replicates. *p* values were calculated using ANOVA combined with Tukey's multiple comparison test (****$p < 0.0001$, ***$p < 0.001$, **$p < 0.01$, *$p < 0.05$).

Figure S5

A

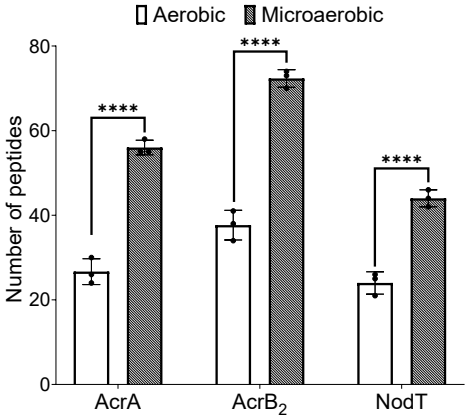

Figure S5: Metabolism switch upon $AcrAB_2NodT$ expression. A. Normalized total spectrum count of $AcrAB_2NodT$ protein in PYE medium, in aerobic and microaerobic conditions. All data are represented as the mean ± SD, with at least three biological replicates. *p* values were calculated using ANOVA combined with Sidak's multiple comparison test (****$p < 0.0001$, ***$p < 0.001$, **$p < 0.01$, *$p < 0.05$).